Theoretical Insights into the Metal−Nonmetal Interaction Inside $M_2O@C_{2v}(31922)$-C_{80} (M = Sc or Gd)

Wenxin Zhang, Mengyang Li, Jun He, and Xiang Zhao*

Read Online

ACCESS | Metrics & More | Article Recommendations | Supporting Information

ABSTRACT: The metal−nonmetal interaction is complicated but significant in organometallic chemistry and metallic catalysis and is susceptible to the coordination surroundings. Endohedral metallofullerene is considered to be an excellent model for studying metal−nonmetal interactions with the shielding effect of fullerenes. Herein, with the detection of ScGdO@C_{80} in a previous mass spectrum, we studied the effects of metal atoms (Sc and Gd) on the metal−nonmetal interactions of the thermodynamically stable molecules $M_2O@C_{2v}(31922)$-C_{80} (M = Sc and Gd), where metal atoms M can be the same or different, using density functional theory calculations. The inner metal atom and the fullerene cage show mainly ionic interactions with some covalent character. The Sc atom with higher electronegativity plays a greater important role in the metal−nonmetal interactions than the Gd atom. This study would be useful for the further study of the metal−nonmetal interaction.
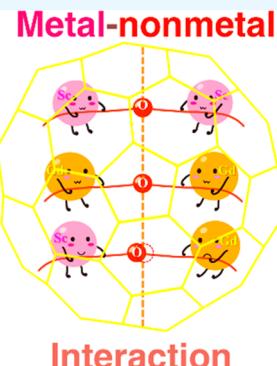
INTRODUCTION

Endohedral metallofullerene (EMF) is a unique carbon nanomaterial in which metal ions, metal atoms, or metal clusters are embedded in fullerene carbon cages. Since the discovery of LaC_{60}, the prototype of EMFs, in 1985,[1] EMFs have attracted much attention because of their unique core−shell structure and promising applications in biomedicine, solar cells, and materials science.[2−7] Additionally, more and more EMFs have been reported, such as $Sc_3N@C_{2n}$ ($2n$ = 68−70 and 78−82),[8−16] $Sc_2C_2@C_{2n}$ ($2n$ = 68, 72−74, and 80−84),[17−22] $Sc_2S@C_{2n}$ ($2n$ = 70 and 82),[23−25] $YCN@C_{82}$,[26] $Sc_3CH@C_{80}$,[27] $Sc_3NC@C_{2n}$ ($2n$ = 78−80),[28,29] and $Sc_2O@C_{2n}$ (n = 35−47).[30−35] According to the types of inner clusters, clusterfullerenes can be classified into nitride clusterfullerene, carbide clusterfullerene, sulfide clusterfullerene, cyanide clusterfullerene, metal hydrocarbon clusterfullerene, metal carbonitride clusterfullerene, and oxide clusterfullerene (OCF).[36] OCFs, including $Sc_2O@C_{2n}$, $Ho_2O@C_{74}$,[37] $Ho_2O@C_{84}$,[38] $Dy_2O@C_{80}$,[39] etc., have been widely studied. In particular, $Sc_2O@C_{2n}$ has attracted much attention since 2010 due to their successful preparation and characterization. The molecular orbital energy levels and internal cluster dynamics of OCFs rely on both the cluster and the carbon cages.[36] In general, with the increase in of the size of the carbon cage, the angle of Sc−O−Sc clusters gradually increases and the M_2O clusters become more disordered. This may be attributed to the strong metal−carbon interaction and the spatial limitation of fullerene cages.[31]

Clusterfullerene is an ideal model for studying the interaction between metals and nonmetals (C, N, and O atoms), which is of great significance for the reasonable design

of metal−organic frameworks and metal catalysts that show promising and excellent applications in dealing with global warming and the energy crisis. In addition, the study of the metal−nonmetal interaction in EMFs is very important to reveal the reaction selectivity and predict the molecular structure and reactivity of EMFs.[40−42] To date, there have been many studies on the metal−nonmetal interaction in the model of clusterfullerenes, but only a few studies on the effect of different metals on the metal−nonmetal interaction in the same fullerene cage. Luckily, Chen et al. isolated a mixed metal oxide cluster fullerene (MMOCF), ScGdO@C_{82}, for the first time in 2018.[43] The mass spectra showed the existence of ScGdO@C_{80}, and $Sc_2O@C_{80}$[32] was prepared previously. Clearly, ScGdO@C_{80} is an excellent prototype to understand the effect of Gd and Sc on the metal−nonmetal interaction. Here, a theoretical study was first carried out on the thermodynamic stability, geometry, and electronic structure of ScGdO@C_{80}. Then, the metal−nonmetal interaction in $M_2O@C_{2v}(31922)$-C_{80} (M = Sc and Gd), where metal atoms M can be the same or different, was studied and compared in detail using density functional theory (DFT) calculations and wave functional analyses. Note that the name of the fullerene cage in references has not been changed with respect to the

original authors, and in this work we use the spiral number to name the fullerene cages.

COMPUTATIONAL DETAILS

The previous study[44] showed the relative stability of anion C_{80}^{4-}, wherein seven lowest-energy tetra-anionic cages (less than ~40 kcal·mol^{-1}) were selected to encase ScGdO. Then, the optimizations of ScGdO@C$_{80}$ were performed at the BP86/6-31G(d)~CEP-4G level of theory,[45−48] where the basis set 6-31G(d) was used for C and O atoms and CEP-4G, including the pseudopotential function, was used for Sc and Gd atoms. The BP86 function has been used to study many EMFs theoretically[32,44,49] with negligible spin contamination. The core electron of the heavy metal atom will not affect the electronic features of metal-based complexes, and the CEP-4G basis function including a pseudopotential can accurately describe the electronic features of Gd. The vibration frequency analysis was carried out at the same theoretical level to confirm that all the stationary points were minimums and free from an imaginary frequency. Furthermore, the results of the single-point calculations at the ωB97X-D/6-31G(d)~CEP-4G level of theory confirm the optimization results at the BP86/6-31G(d)~CEP-4G level of theory, indicating the rationality of the theoretical levels in the present work. Based on the structure and vibration data, the relative concentration of ScGdO@C$_{80}$ and the enthalpy−entropy effect were calculated, which is a reliable method of evaluating the thermodynamic stability of EMFs in the fullerene-formation temperature region.[50−52] The interaction energies of ScGdO@C$_{80}$, Sc$_2$O@C$_{80}$, and Gd$_2$O@C$_{80}$ were also calculated to elucidate their relative stabilities. Their electronic structures were studied by natural population analysis, and infrared (IR) spectra were also simulated to give more information to help characterize the structures experimentally. All the above DFT calculations in this work were performed with the Gaussian 16 program.[53] The Mayer bond order analysis, the DOS, and the BCP analysis were based on the results of the geometric optimization and frequency calculation at the BP86/6-31G(d)~CEP-4G level of theory and were carried out with Multifwn program[54] to study the interactions between metal and nonmetal atoms.

RESULTS AND DISCUSSION

According to the ionic model of EMFs, the seven low-lying C_{80}^{4-} anions were selected to encage ScGdO cluster.[44] After the encapsulations, IPR ScGdO@C_{2v}(31922)-C$_{80}$ possesses the lowest potential energy, followed by IPR ScGdO@I_h(31924)-C$_{80}$ and ScGdO@D_{5h}(31923)-C$_{80}$ with higher relative energies of 2.4 and 6.0 kcal·mol^{-1}, respectively, as shown in Table S1. Additionally, because of the electron transfer, the energy gaps between the singly occupied molecular orbital (SOMO) and the lowest unoccupied molecular orbital (LUMO) of the ScGdO@C$_{80}$ isomers (Figure S1) decreased after the encapsulation compared with those of the C_{80}^{4-} anions.[44] The energies of the single-point calculations at the ωB97X-D level of theory also indicate that ScGdO@C_{2v}(31922)-C$_{80}$ has the lowest relative energy (Table S1). As shown in Figure 1, the statistical thermodynamic analysis of ScGdO@C$_{80}$ isomers, including the enthalpy−entropy effects, confirmed the highest concentration of ScGdO@C_{2v}(31922)-C$_{80}$ in the whole temperature region, followed by ScGdO@I_h(31924)-C$_{80}$ and ScGdO@
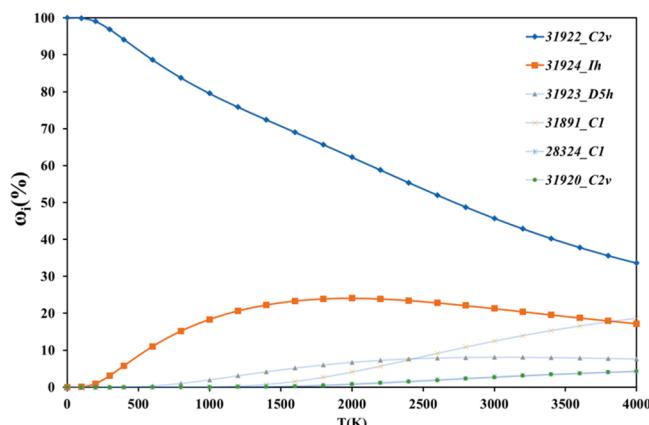

Figure 1. Relative concentrations of several low-lying isomers of ScGdO@C$_{80}$ at the BP86/6-31G(d)~CEP-4G level of theory.


ScGdO@C_{2v}(31922)-C$_{80}$ Sc$_2$O@C_{2v}(31922)-C$_{80}$ Gd$_2$O@C_{2v}(31922)-C$_{80}$
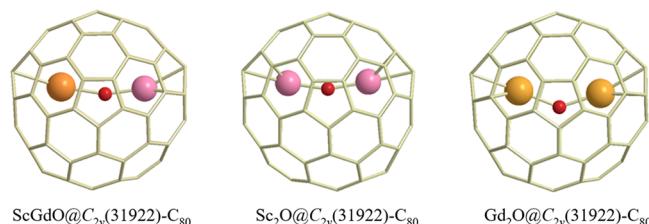
Figure 2. Geometry structures of ScGdO@C_{2v}(31922)-C$_{80}$, Sc$_2$O@C_{2v}(31922)-C$_{80}$, and Gd$_2$O@C_{2v}(31922)-C$_{80}$ optimized at the BP86/6-31G(d)~CEP-4G level of theory. Oxygen, scandium, and gadolinium atoms are colored in red, pink, and orange, respectively.

Table 1. Natural Electron Configuration Populations of O, Sc, and Gd atoms in ScGdO@C_{2v}(31922)-C$_{80}$, Sc$_2$O@C_{2v}(31922)-C$_{80}$, and Gd$_2$O@C_{2v}(31922)-C$_{80}$ at the BP86/6-31G(d)~CEP-4G Level of Theory

isomer	atom	NBO charge	population
ScGdO@C_{2v}(31922)-C$_{80}$	O81	−1.091	2s$^{1.79}$2p$^{5.30}$
	Sc82	1.436	3d$^{0.68}$4s$^{0.07}$4p$^{0.36}$
	Gd83	1.863	4f$^{7.02}$5d$^{0.88}$6s$^{0.07}$6p$^{0.20}$
Sc$_2$O@C_{2v}(31922)-C$_{80}$	O81	−1.204	2s$^{1.82}$2p$^{5.37}$
	Sc82	1.891	3d$^{0.63}$4s$^{0.01}$4p$^{0.36}$
	Sc83	1.898	3d$^{0.64}$4s$^{0.01}$4p$^{0.35}$
Gd$_2$O@C_{2v}(31922)-C$_{80}$	O81	−1.463	2s$^{1.93}$2p$^{5.52}$
	Gd82	2.368	4f$^{7.03}$5d$^{0.53}$6s$^{0.03}$6p$^{0.07}$
	Gd83	2.375	4f$^{7.03}$5d$^{0.53}$6s$^{0.02}$6p$^{0.07}$

D_{5h}(31923)-C$_{80}$ with highest concentrations of no more than 24.1% and 10%, respectively, below about 2500 K; this showed that ScGdO@C_{2v}(31922)-C$_{80}$ had the highest thermodynamic stability. The accuracy of this theoretical method has been confirmed in many experiments, such as those for Sc$_2$O@T_d(19151)-C$_{76}$, Sc$_2$O@C_{2v}(5)-C$_{80}$, Sc$_2$O@C_s(6)-C$_{82}$, and Sc$_2$O@C_{3v}(8)-C$_{82}$.[32−34,55]

Besides, Sc$_2$O@C_{2v}(5)-C$_{80}$ has been isolated[32] with the same carbon cage as optimal ScGdO@C_{2v}(31922)-C$_{80}$. To elucidate the effect of inner metal atoms on M$_2$O@C$_{2n}$ (M = Sc and Gd), including the metal−nonmetal interactions, crystallized Sc$_2$O@C_{2v}(31922)-C$_{80}$ and the Gd$_2$O@C_{2v}(31922)-C$_{80}$ model were optimized at the same theoretical level used for the optimization of ScGdO@C_{2v}(31922)-C$_{80}$. The interaction energies (E) in ScGdO@C_{2v}(31922)-C$_{80}$, Sc$_2$O@C_{2v}(31922)-C$_{80}$, and Gd$_2$O@C_{2v}(31922)-C$_{80}$ between inner metal oxides
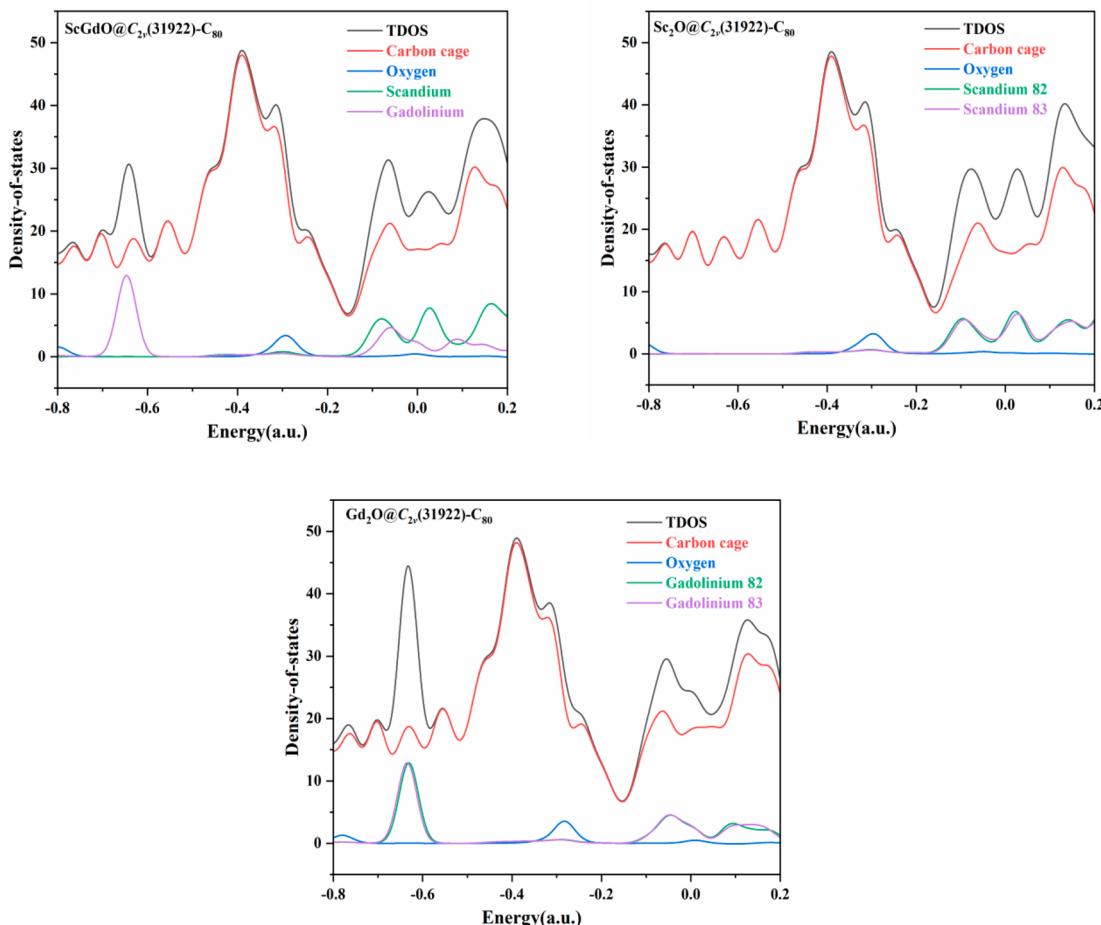
Figure 3. TDOS and PDOS of ScGdO@C_{2v}(31922)-C_{80}, Sc$_2$O@C_{2v}(31922)-C_{80}, and Gd$_2$O@C_{2v}(31922)-C_{80}.

ScGdO@C_{2v}(31922)-C_{80} Sc$_2$O@C_{2v}(31922)-C_{80} Gd$_2$O@C_{2v}(31922)-C_{80}
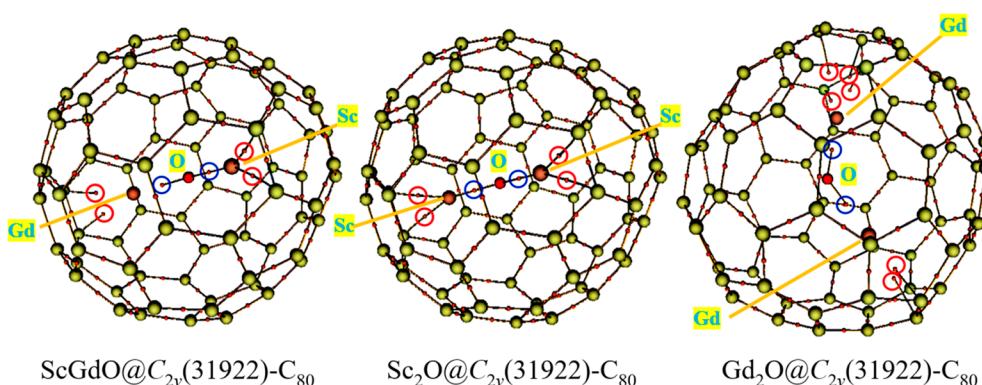
Figure 4. BCPs in ScGdO@C_{2v}(31922)-C_{80}, Sc$_2$O@C_{2v}(31922)-C_{80}, and Gd$_2$O@C_{2v}(31922)-C_{80}. BCPs are represented in orange, and BCP paths are represented as brown sticks. BCPs between metal atoms and the carbon cage are highlighted in red, and those between metal atoms and O atoms are circled in blue.

and C_{2v}(31922)-C_{80} are −167.9, −172.3, and −178.2 kcal·mol^{-1}, respectively, indicating the thermodynamically maintained present configurations; the interaction energy was calculated using $E = E_{EMF} - E_{carbon-cage} - E_{cluster}$. The energies of EMFs ($E_{EMF}$) were obtained by the optimization of EMFs, and the energies of the singlet-ground-state carbon cage ($E_{carbon-cage}$) and the inner cluster ($E_{cluster}$, octet-ground state ScGdO, singlet-ground-state Sc$_2$O, and 15-et-ground-state Gd$_2$O) were obtained from the single-point calculations of the carbon cage and the inner cluster from the corresponding optimized EMFs, respectively. ScGdO@C_{2v}(31922)-C_{80} has

the largest interaction energy, indicating its lower thermodynamically stability; thus, it is a bit difficult to isolate and crystallize ScGdO@C_{2v}(31922)-C_{80}, likely because of its asymmetric geometry.

As shown in Figures 2 and S2, the Sc−O bond length in ScGdO@C_{2v}(31922)-C_{80} is 1.889 Å, which is shorter than the length of the Gd−O bond (2.113 Å). The greater electronegativity of Sc possibly leads to this result. Surprisingly, both distances are slightly larger than those (1.859 and 2.056 Å for Sc−O and Gd−O bonds, respectively) in ScGdO@C_{3v}(8)-C_{82}[43] with larger fullerene cages, which is derived from the

Table 2. BCP Parameters of Clusters and Cluster−Cage Interactions in ScGdO@C_{2v}(31922)-C_{80}, Sc_2O@C_{2v}(31922)-C_{80}, and Gd_2O@C_{2v}(31922)-C_{80} [a]

bond	d (Å)	ρ_{BCP}	$\nabla^2\rho_{BCP}$	H_{BCP}	$|V_{BCP}|/G_{BCP}$	ε	MBO
ScGdO@C_{2v}(31922)-C_{80}							
Sc82−C51	2.304	0.054	0.202	−0.004	1.080	1.158	0.242
Sc82−C52	2.305	0.054	0.202	−0.004	1.079	1.240	0.242
Sc82−O81	1.889	0.122	0.623	−0.020	1.113	0.009	1.194
Gd83−C71	2.524	0.048	0.163	−0.004	1.090	0.748	0.169
Gd83−C72	2.525	0.048	0.162	−0.004	1.090	0.789	0.169
Gd83−O81	2.113	0.098	0.434	−0.012	1.101	0.001	0.685
Sc_2O@C_{2v}(31922)-C_{80}							
Sc82−C51	2.345	0.050	0.187	−0.003	1.061	1.534	0.208
Sc82−C52	2.344	0.050	0.187	−0.003	1.062	1.489	0.209
Sc82−O81	1.924	0.111	0.575	−0.014	1.088	0.006	1.009
Sc83−C71	2.316	0.053	0.195	−0.004	1.081	1.188	0.229
Sc83−C72	2.321	0.053	0.194	−0.004	1.078	1.362	0.229
Sc83−O81	1.960	0.100	0.525	−0.008	1.059	0.016	0.922
Gd_2O@C_{2v}(31922)-C_{80}							
Gd82−C71	2.497	0.050	0.172	−0.005	1.103	0.737	0.170
Gd82−C72	2.496	0.050	0.173	−0.005	1.103	0.715	0.170
Gd82−O81	2.067	0.110	0.488	−0.019	1.136	0.015	0.886
Gd83−C47	2.581	0.042	0.146	−0.002	1.054	2.142	0.162
Gd83−C44	2.582	0.042	0.146	−0.002	1.054	2.192	0.162
Gd83−C52	2.557	0.045	0.156	−0.003	1.074	1.190	0.153
Gd83−C51	2.556	0.045	0.156	−0.003	1.074	1.159	0.153
Gd83−O81	2.053	0.114	0.498	−0.022	1.150	0.013	0.917

[a]The units of all the BCP parameters are Å and a.u.
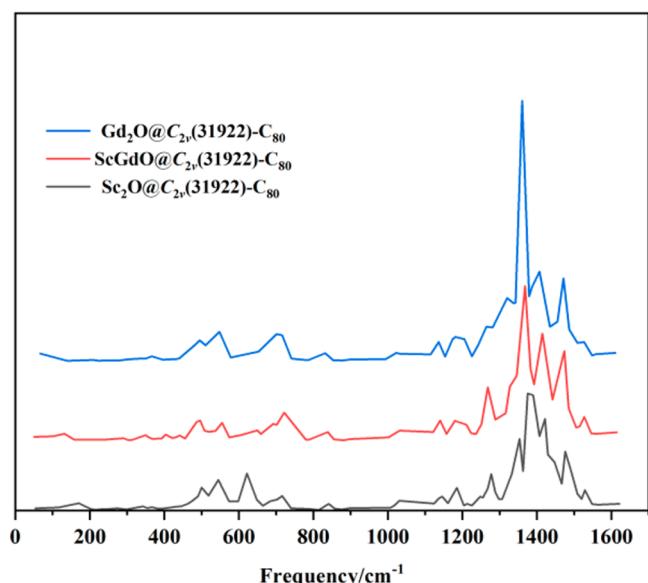
Figure 5. Infrared spectra of thermodynamically stable ScGdO@ C_{2v}(31922)-C_{80}, Sc_2O@C_{2v}(31922)-C_{80}, and Gd_2O@C_{2v}(31922)-C_{80} at the BP86/6-31G(d)∼CEP-4G level of theory.

orientation of the inner ScGdO cluster along the short axis of C_{3v}(8)-C_{82}.

Additionally, the Sc−O and Gd−O bond lengths are 1.924 and 2.053 Å in Sc_2O@C_{2v}(31922)-C_{80} and 1.960 and 2.067 Å in Gd_2O@C_{2v}(31922)-C_{80}, respectively. The Sc−O−Gd angle (163.0°) is larger than the Sc−O−Sc angle (161.7°) and the Gd−O−Gd angle (139.9°) in Sc_2O@C_{2v}(31922)-C_{80} and Gd_2O@C_{2v}(31922)-C_{80}, respectively. These results show the more serious effect of the Sc metal atom on the geometries of metal oxide fullerenes compared to the Gd metal atom, which

further illustrates the influence of the electronegativity of the Sc atom.

To further understand the effect of the metal atom on electronic structures, natural bond orbital (NBO) calculations were performed (Table 1). Based on the ground-state electronic configurations of the Sc ($3d^14s^2$) and Gd ($4f^75d^16s^2$) atoms and the spin electronic population of ScGdO@C_{2v}(31922)-C_{80} in the octet ground state (Figure S3 and Table S2), the formal oxidation states of inner Sc and Gd atoms are III. In the similar way, the formal oxidation states of Sc and Gd in singlet-ground-state Sc_2O@C_{2v}(31922)-C_{80} and 15-et-ground-state Gd_2O@C_{2v}(31922)-C_{80} are also III. The spin ground state of Sc_2O@C_{2v}(31922)-C_{80} was calculated previously,[32] and we inferred the spin state of Gd_2O@ C_{2v}(31922)-C_{80} from the other two isomers. The NBO charge is negative for the O atom and positive for the metal atom, which shows there is electron transfer from metal atoms to the O atom. In ScGdO@C_{2v}(31922)-C_{80}, the NBO charge of the O atom is less negative and the two metals are quite different. Because of the f orbital, the Gd atoms seem to lose electrons more easily. The partial charge in outer s, p, and d orbitals is derived from back-donation from the O atom and the fullerene cage, indicating the covalent features between metal and nonmetal atoms; these features were also confirmed by the density of states (Figure 3). The large difference in atomic charge between Sc and Gd is attributed to their electronegativity. According to the eight-electron rule of the O atom, the formal four-electron transfer occurs from the inner cluster (ScGdO, Sc_2O, and Gd_2O) to C_{2v}(31922)-C_{80}.

Bonding critical point (BCP) indicators based on the quantum theory of atoms in molecules (QTAIM, a mature quantum theory for analyzing the topology of the electron density) were studied (Figure 4) to further determine the metal−nonmetal interactions. As shown in Table 2, the BCP

indicators between Sc(Gd) and carbon atoms have similar values. The density of electrons (ρ_{BCP}) is small, and the Laplacian of electron density ($\nabla^2\rho_{BCP}$) is positive, in line with the previous results on EMFs.[56,57] Low ρ_{BCP} values, positive $\nabla^2\rho_{BCP}$ values, energy density (H_{BCP}) close to zero, and low Mayer bond orders (MBOs) show the ionic interaction between metal and nonmetal atoms. The larger than 1 ratio between the absolute value of the potential energy density and the kinetic energy density ($|V_{BCP}|/G_{BCP}$) indicates the interaction consists of an ionic interaction and a covalent interaction, and the negative H_{BCP} value is the symbol of the covalent interaction. Therefore, the metal−nonmetal interaction inside $M_2O@C_{2v}(31922)$-C_{80} (M = Sc or Gd) is mainly an ionic interaction with some covalent character. Because of larger ρ_{BCP}, more negative H_{BCP}, larger $|V_{BCP}|/G_{BCP}$, larger MBO, and shorter atom distance, the Sc−O and Sc−C interactions are stronger than the Gd−O and Gd−C interactons in ScGdO@$C_{2v}(31922)$-C_{80}, which may be attributed to the higher electronegativity of the Sc atom. Compared with $Sc_2O@C_{2v}(31922)$-C_{80}, Table 2 shows that the Sc−O interaction in ScGdO@$C_{2v}(31922)$-C_{80} is stronger according to the BCP indicators. In contrast, the Gd−O interaction in ScGdO@$C_{2v}(31922)$-C_{80} is weaker than that in $Gd_2O@C_{2v}(31922)$-C_{80}. This phenomenon is likely related to (1) the difference in electronegativity determining the electron-withdrawing ability, (2) the atomic orbital energy level determining the degree of effective overlap between bonding atoms, and (3) the size of the atomic radius. Additionally, close to zero bond ellipticity values between Sc or Gd and O atoms indicate single bonds, confirming the four-electron transfer phenomenon. Replacing the Sc atom with the Gd atom in $Sc_2O@C_{2v}(31922)$-C_{80} makes the Sc−C interaction (Sc82−C51 and Sc82−C52) stronger; interestingly, however, substituting the Sc atom for the Gd atom in $Gd_2O@C_{2v}(31922)$-C_{80} makes the Gd−C (Gd82−C71 and Gd82−C72) interaction weaker.

To give some useful structural information to distinguish similar molecules of ScGdO@$C_{2v}(31922)$-C_{80}, $Sc_2O@C_{2v}(31922)$-C_{80}, and $Gd_2O@C_{2v}(31922)$-C_{80} in future experiments, their infrared spectra were simulated, as shown in Figure 5. These three kinds of EMFs have very similar absorption peaks. The absorption peak between 200 and 800 cm^{-1} is the vibration of the fullerene frame. The absorption peaks above 1000 cm^{-1} come from the stretching vibration of the C−C bond. For higher numbers of Gd atoms, the strongest absorption peak is slightly red shifted, which is meaningful for their experimental characterization.

CONCLUSION

Using density functional theory and statistical thermodynamic analysis, ScGdO@$C_{2v}(31922)$-C_{80} was found to be the most likely isomer isolated in the experiment. The comparative study on $Sc_2O@C_{2v}(31922)$-C_{80} and $Gd_2O@C_{2v}(31922)$-C_{80} shows that ScGdO@$C_{2v}(31922)$-C_{80} has the largest bond angle because of its stronger interaction between metal and carbon atoms, and the Sc atom with higher electronegativity plays a much more important role in the metal−nonmetal interactions than the Gd atom. The interactions of Sc−O and Sc−C are larger than those of Gd−C and Gd−O, which is likely related to the higher electronegativity of the Sc atoms and the much closer orbital energy levels. Finally, IR spectra of three isomers were simulated to help future experimental research.

ASSOCIATED CONTENT

ⓢ Supporting Information

The Supporting Information is available free of charge at https://pubs.acs.org/doi/10.1021/acsomega.2c04978.

Relative energies, single-point energies, relative concentrations, spin density maps, structures for BCPs, BCP parameters, TDOS and PDOS, SOMO- and HOMO−LUMO gaps and maps, and Cartesian coordinates of $M_2O@C_{80}$ (M = Sc or Gd) (PDF)

AUTHOR INFORMATION

Corresponding Author

Xiang Zhao − Institute of Molecular Science and Applied Chemistry, School of Chemistry, State Key Laboratory of Electrical Insulation and Power Equipment, and MOE Key Laboratory for Nonequilibrium Synthesis and Modulation of Condensed Matter, Xi'an Jiaotong University, Xi'an, Shaanxi 710049, China; ⓞ orcid.org/0000-0003-3982-4763; Email: xzhao@mail.xjtu.edu.cn

Authors

Wenxin Zhang − Institute of Molecular Science and Applied Chemistry, School of Chemistry, State Key Laboratory of Electrical Insulation and Power Equipment, and MOE Key Laboratory for Nonequilibrium Synthesis and Modulation of Condensed Matter, Xi'an Jiaotong University, Xi'an, Shaanxi 710049, China

Mengyang Li − School of Physics, Xidian University, Xi'an, Shaanxi 710071, China

Jun He − Institute of Molecular Science and Applied Chemistry, School of Chemistry, State Key Laboratory of Electrical Insulation and Power Equipment, and MOE Key Laboratory for Nonequilibrium Synthesis and Modulation of Condensed Matter, Xi'an Jiaotong University, Xi'an, Shaanxi 710049, China

Complete contact information is available at:
https://pubs.acs.org/10.1021/acsomega.2c04978

Author Contributions

W.X.Z. and M.Y.L. contributed equally to this work.

Notes

The authors declare no competing financial interest.

ACKNOWLEDGMENTS

REFERENCES

(1) Heath, J. R.; O'Brien, S. C.; Zhang, Q.; Liu, Y.; Curl, R. F.; Tittel, F. K.; Smalley, R. E. Lanthanum Complexes of Spheroidal Carbon Shells. J. Am. Chem. Soc. 1985, 107, 7779−7780.

(2) Popov, A. A.; Yang, S. F.; Dunsch, L. Endohedral Fullerenes. Chem. Rev. 2013, 113, 5989−6113.

(3) Lu, X.; Bao, L. P.; Akasaka, T.; Nagase, S. Recent Progress in the Chemistry of Endohedral Metallofullerenes. Chem. Commun. 2014, 50, 14701−14715.

(4) Liu, Y.; Jiao, F.; Qiu, Y.; Li, W.; Lao, F.; Zhou, G. Q.; Sun, B. Y.; Xing, G. M.; Dong, J. Q.; Zhao, Y. L.; Chai, Z. F.; Chen, C. Y. The

Effect of Gd@C$_{82}$(OH)$_{22}$ Nanoparticles on the Release of Th1/Th2 Cytokines and Induction of TNF-A Mediated Cellular Immunity. *Biomaterials* **2009**, *30*, 3934−3945.

(5) Wang, J.; Hu, Z. B.; Xu, J. X.; Zhao, Y. L. Therapeutic Applications of Low-Toxicity Spherical Nanocarbon Materials. *NPG Asia Mater.* **2014**, *6*, e84.

(6) Li, J.; Zhao, F. W.; Wang, T. S.; Nie, M. Z.; Li, J. J.; Wei, Z. X.; Jiang, L.; Wang, C. R. Ethylenediamine Functionalized Fullerene Nanoparticles as Independent Electron Transport Layers for High-Efficiency Inverted Polymer Solar Cells. *J. Mater. Chem.A* **2017**, *5*, 947−951.

(7) Nagano, T.; Kuwahara, E.; Takayanagi, T.; Kubozono, Y.; Fujiwara, A. Fabrication and Characterization of Field-Effect Transistor Device with C$_{2v}$ Isomer of Pr@C$_{82}$. *Chem. Phys. Lett.* **2005**, *409*, 187−191.

(8) Hino, S.; Ogasawara, N.; Ohta, T.; Yagi, H.; Miyazaki, T.; Nishi, T.; Shinohara, H. Electronic Structure of Sc$_3$N@C$_{68}$. *Chem. Phys.* **2013**, *421*, 39−43.

(9) Yang, S. F.; Popov, A. A.; Dunsch, L. Violating the Isolated Pentagon Rule (IPR): The Endohedral Non-IPR C$_{70}$ Cage of Sc$_3$N@C$_{70}$. *Angew. Chem., Int. Ed.* **2007**, *46*, 1256−1259.

(10) Campanera, J. M.; Bo, C.; Olmstead, M. M.; Balch, A. L.; Poblet, J. M. Bonding within the Endohedral Fullerenes Sc$_3$N@C$_{78}$ and Sc$_3$N@C$_{80}$ as Determined by Density Functional Calculations and Reexamination of the Crystal Structure of {Sc$_3$N@C$_{78}$}· Co(OEP)·1.5(C$_6$H$_6$)·0.3(CHCl$_3$). *J. Phys. Chem. A* **2002**, *106*, 12356−12364.

(11) Krause, M.; Popov, A.; Dunsch, L. Vibrational Structure of Endohedral Fullerene Sc$_3$N@C$_{78}$ (*D$_{3h}$* '): Evidence for a Strong Coupling between the Sc$_3$N Cluster and C$_{78}$ Cage. *ChemPhysChem* **2006**, *7*, 1734−1740.

(12) Cai, T.; Xu, L.; Gibson, H. W.; Dorn, H. C.; Chancellor, C. J.; Olmstead, M. M.; Balch, A. L. Sc$_3$N@C$_{78}$: Encapsulated Cluster Regiocontrol of Adduct Docking on an Ellipsoidal Metallofullerene Sphere. *J. Am. Chem. Soc.* **2007**, *129*, 10795−10800.

(13) Stevenson, S.; Rice, G.; Glass, T.; Harich, K.; Cromer, F.; Jordan, M. R.; Craft, J.; Hadju, E.; Bible, R.; Olmstead, M. M.; Maitra, K.; Fisher, A. J.; Balch, A. L.; Dorn, H. C. Small-Bandgap Endohedral Metallofullerenes in High Yield and Purity. *Nature* **1999**, *402*, 898−898.

(14) Stevenson, S.; Lee, H. M.; Olmstead, M. M.; Kozikowski, C.; Stevenson, P.; Balch, A. L. Preparation and Crystallographic Characterization of a New Endohedral, Lu$_3$N@C$_{80}$·5(*o*-xylene), and Comparison with Sc$_3$N@C$_{80}$·5(*o*-xylene). *Chem. Eur. J.* **2002**, *8*, 4528−4535.

(15) Lee, H. M.; Olmstead, M. M.; Iezzi, E.; Duchamp, J. C.; Dorn, H. C.; Balch, A. L. Crystallographic Characterization and Structural Analysis of the First Organic Functionalization Product of the Endohedral Fullerene Sc$_3$N@C$_{80}$. *J. Am. Chem. Soc.* **2002**, *124*, 3494−3495.

(16) Wei, T.; Wang, S.; Liu, F. P.; Tan, Y. Z.; Zhu, X. J.; Xie, S. Y.; Yang, S. F. Capturing the Long-Sought Small-Bandgap Endohedral Fullerene Sc$_3$N@C$_{82}$ with Low Kinetic Stability. *J. Am. Chem. Soc.* **2015**, *137*, 3119−3123.

(17) Shi, Z. Q.; Wu, X.; Wang, C. R.; Lu, X.; Shinohara, H. Isolation and Characterization of Sc$_2$C$_2$@C$_{68}$: A Metal-Carbide Endofullerene with a Non-IPR Carbon Cage. *Angew. Chem., Int. Ed.* **2006**, *45*, 2107−2111.

(18) Feng, Y. Q.; Wang, T. S.; Wu, J. Y.; Feng, L.; Xiang, J. F.; Ma, Y. H.; Zhang, Z. X.; Jiang, L.; Shu, C. Y.; Wang, C. R. Structural and Electronic Studies of Metal Carbide Clusterfullerene Sc$_2$C$_2$@C$_s$-C$_{72}$. *Nanoscale* **2013**, *5*, 6704−6707.

(19) Wang, Y. F.; Tang, Q. Q.; Feng, L.; Chen, N. Sc$_2$C$_2$@ *D$_{3h}$*(14246)-C$_{74}$: A Missing Piece of the Clusterfullerene Puzzle. *Inorg. Chem.* **2017**, *56*, 1974−1980.

(20) Kurihara, H.; Lu, X.; Iiduka, Y.; Mizorogi, N.; Slanina, Z.; Tsuchiya, T.; Akasaka, T.; Nagase, S. Sc$_2$C$_2$@C$_{80}$ Rather Than Sc$_2$@ C$_{82}$: Templated Formation of Unexpected C$_{2v}$(5)-C$_{80}$ and Temper-ature-Dependent Dynamic Motion of Internal Sc$_2$C$_2$ Cluster. *J. Am. Chem. Soc.* **2011**, *133*, 2382−2385.

(21) Kurihara, H.; Lu, X.; Iiduka, Y.; Nikawa, H.; Hachiya, M.; Mizorogi, N.; Slanina, Z.; Tsuchiya, T.; Nagase, S.; Akasaka, T. X-Ray Structures of Sc$_2$C$_2$@C$_{2n}$ (*n* = 40−42): In-Depth Understanding of the Core-Shell Interplay in Carbide Cluster Metallofullerenes. *Inorg. Chem.* **2012**, *51*, 746−750.

(22) Yamazaki, Y.; Nakajima, K.; Wakahara, T.; Tsuchiya, T.; Ishitsuka, M. O.; Maeda, Y.; Akasaka, T.; Waelchli, M.; Mizorogi, N.; Nagase, S. Observation of ^{13}C NMR Chemical Shifts of Metal Carbides Encapsulated in Fullerenes: Sc$_2$C$_2$@C$_{82}$, Sc$_2$C$_2$@C$_{84}$, and Sc$_3$C$_2$@C$_{80}$. *Angew. Chem., Int. Ed.* **2008**, *47*, 7905−7908.

(23) Chen, N.; Mulet-Gas, M.; Li, Y. Y.; Stene, R. E.; Atherton, C. W.; Rodriguez-Fortea, A.; Poblet, J. M.; Echegoyen, L. Sc$_2$S@ C$_2$(7892)-C$_{70}$: A Metallic Sulfide Cluster inside a Non-IPR C$_{70}$ Cage. *Chem. Sci.* **2013**, *4*, 180−186.

(24) Chen, N.; Chaur, M. N.; Moore, C.; Pinzon, J. R.; Valencia, R.; Rodriguez-Fortea, A.; Poblet, J. M.; Echegoyen, L. Synthesis of a New Endohedral Fullerene Family, Sc$_2$S@C$_{2n}$ (*n* = 40−50) by the Introduction of SO$_2$. *Chem. Commun.* **2010**, *46*, 4818−4820.

(25) Mercado, B. Q.; Chen, N.; Rodriguez-Fortea, A.; Mackey, M. A.; Stevenson, S.; Echegoyen, L.; Poblet, J. M.; Olmstead, M. M.; Balch, A. L. The Shape of the Sc$_2$(μ $_2$-S) Unit Trapped in C$_{82}$: Crystallographic, Computational, and Electrochemical Studies of the Isomers, Sc$_2$(μ $_2$-S)@C$_s$(6)-C$_{82}$ and Sc$_2$(μ $_2$-S)@C$_{3v}$(8)-C$_{82}$. *J. Am. Chem. Soc.* **2011**, *133*, 6752−6760.

(26) Yang, S. F.; Chen, C. B.; Liu, F. P.; Xie, Y. P.; Li, F. Y.; Jiao, M. Z.; Suzuki, M.; Wei, T.; Wang, S.; Chen, Z. F.; Lu, X.; Akasaka, T. An Improbable Monometallic Cluster Entrapped in a Popular Fullerene Cage: YCN@C$_s$(6)-C$_{82}$. *Sci. Rep* **2013**, *3*, 1487.

(27) Krause, M.; Ziegs, F.; Popov, A. A.; Dunsch, L. Entrapped Bonded Hydrogen in a Fullerene: The Five-Atom Cluster Sc$_3$CH in C$_{80}$. *ChemPhysChem* **2007**, *8*, 537−540.

(28) Wu, J. Y.; Wang, T. S.; Ma, Y. H.; Jiang, L.; Shu, C. Y.; Wang, C. R. Synthesis, Isolation, Characterization, and Theoretical Studies of Sc$_3$NC@C$_{78}$-C$_2$. *J. Phys. Chem. C* **2011**, *115*, 23755−23759.

(29) Wang, T. S.; Feng, L.; Wu, J. Y.; Xu, W.; Xiang, J. F.; Tan, K.; Ma, Y. H.; Zheng, J. P.; Jiang, L.; Lu, X.; Shu, C. Y.; Wang, C. R. Planar Quinary Cluster inside a Fullerene Cage: Synthesis and Structural Characterizations of Sc$_3$NC@C$_{80}$-*I$_h$*. *J. Am. Chem. Soc.* **2010**, *132*, 16362−16364.

(30) Zhang, M. R.; Hao, Y. J.; Li, X. H.; Feng, L.; Yang, T.; Wan, Y. B.; Chen, N.; Slanina, Z.; Uhlik, F.; Cong, H. L. Facile Synthesis of an Extensive Family of Sc$_2$O@C$_{2n}$(*n* = 35−47) and Chemical Insight into the Smallest Member of Sc$_2$O@C$_2$(7892)-C$_{70}$. *J. Phys. Chem. C* **2014**, *118*, 28883−28889.

(31) Feng, L.; Hao, Y. J.; Liu, A. L.; Slanina, Z. Trapping Metallic Oxide Clusters inside Fullerene Cages. *Acc. Chem. Res.* **2019**, *52*, 1802−1811.

(32) Tang, Q. Q.; Abella, L.; Hao, Y. J.; Li, X. H.; Wan, Y. B.; Rodriguez-Fortea, A.; Poblet, J. M.; Feng, L.; Chen, N. Sc$_2$O@C$_{2v}$(5)-C$_{80}$: Dimetallic Oxide Cluster inside a C$_{80}$ Fullerene Cage. *Inorg. Chem.* **2015**, *54*, 9845−9852.

(33) Tang, Q.; Abella, L.; Hao, Y.; Li, X.; Wan, Y.; Rodriguez-Fortea, A.; Poblet, J. M.; Feng, L.; Chen, N. Sc$_2$O@C$_{3v}$(8)-C$_{82}$: A Missing Isomer of Sc$_2$O@C$_{82}$. *Inorg. Chem.* **2016**, *55*, 1926−1933.

(34) Yang, T.; Hao, Y. J.; Abella, L.; Tang, Q. Q.; Li, X. H.; Wan, Y. B.; Rodriguez-Fortea, A.; Poblet, J. M.; Feng, L.; Chen, N. Sc$_2$O@ *T$_d$*(19151)-C$_{76}$: Hindered Cluster Motion inside a Tetrahedral Carbon Cage Probed by Crystallographic and Computational Studies. *Chem. Eur. J.* **2015**, *21*, 11110−11117.

(35) Zhao, P.; Li, M. Y.; Guo, Y. J.; Zhao, R. S.; Zhao, X. Single Step Stone-Wales Transformation Linking Two Thermodynamically Stable Sc$_2$O@C$_{78}$ Isomers. *Inorg. Chem.* **2016**, *55*, 2220−2226.

(36) Yang, S. F.; Wei, T.; Jin, F. When Metal Clusters Meet Carbon Cages: Endohedral Clusterfullerenes. *Chem. Soc. Rev.* **2017**, *46*, 5005−5058.

(37) Liu, A.; Nie, M. Z.; Hao, Y. J.; Yang, Y.; Wang, T. S.; Slanina, Z.; Cong, H. L.; Feng, L.; Wang, C. R.; Uhlik, F. Ho$_2$O@C$_{74}$: Ho$_2$O

Cluster Expands within a Small Non-IPR Fullerene Cage of $C_2(13333)$-C_{74}. *Inorg. Chem.* **2019**, *58*, 4774−4781.

(38) Cong, H. L.; Liu, A.; Hao, Y. J.; Feng, L.; Slanina, Z.; Uhlik, F. Ho$_2$O@C$_{84}$: Crystallographic Evidence Showing Linear Metallic Oxide Cluster Encapsulated in IPR Fullerene Cage of $D_{2d}(51591)$-C_{84}. *Inorg. Chem.* **2019**, *58*, 10905−10911.

(39) Velkos, G.; Yang, W.; Yao, Y. R.; Sudarkova, S. M.; Liu, F. P.; Avdoshenko, S. M.; Chen, N.; Popov, A. A. Metallofullerene Single-Molecule Magnet Dy$_2$O@C$_{2v}(5)$-C$_{80}$ with a Strong Antiferromagnetic Dy⋯Dy Coupling. *Chem. Commun.* **2022**, *58*, 7164−7167.

(40) Osuna, S.; Swart, M.; Sola, M. The Reactivity of Endohedral Fullerenes. What Can Be Learnt from Computational Studies? *Phys. Chem. Chem. Phys.* **2011**, *13*, 3585−3603.

(41) Garcia-Borras, M.; Osuna, S.; Luis, J. M.; Swart, M.; Sola, M. The Role of Aromaticity in Determining the Molecular Structure and Reactivity of (Endohedral Metallo)Fullerenes. *Chem. Soc. Rev.* **2014**, *43*, 5089−5105.

(42) Li, M. Y.; Zhao, R. S.; Dang, J. S.; Zhao, X. Theoretical Study on the Stabilities, Electronic Structures, and Reaction and Formation Mechanisms of Fullerenes and Endohedral Metallofullerenes. *Coord. Chem. Rev.* **2022**, *471*, 214762.

(43) Yang, W.; Abella, L.; Wang, Y. F.; Li, X. H.; Gu, J. L.; Poblet, J. M.; Rodriguez-Fortea, A.; Chen, N. Mixed Dimetallic Cluster Fullerenes: ScGdO@C$_{3v}(8)$-C$_{82}$ and ScGdC$_2$@C$_{2v}(9)$-C$_{82}$. *Inorg. Chem.* **2018**, *57*, 11597−11605.

(44) Zhao, Y. X.; Li, M. Y.; Zhao, P.; Ehara, M.; Zhao, X. New Insight into U@C$_{80}$: Missing U@$D_3(31921)$-C$_{80}$ and Nuanced Enantiomers of U@$C_1(28324)$-C$_{80}$. *Inorg. Chem.* **2019**, *58*, 14159−14166.

(45) Becke, A. D. Density-Functional Exchange-Energy Approximation with Correct Asymptotic-Behavior. *Phys. Rev. A* **1988**, *38*, 3098−3100.

(46) Perdew, J. P. Density-Functional Approximation for the Correlation-Energy of the Inhomogeneous Electron-Gas. *Phys. Rev. B* **1986**, *33*, 8822−8824.

(47) Cundari, T. R.; Stevens, W. J. Effective Core Potential Methods for the Lanthanides. *J. Chem. Phys.* **1993**, *98*, 5555−5565.

(48) Rassolov, V. A.; Pople, J. A.; Ratner, M. A.; Windus, T. L. 6-31G* Basis Set for Atoms K through Zn. *J. Chem. Phys.* **1998**, *109*, 1223−1229.

(49) Zhang, X. X.; Wang, Y. F.; Morales-Martinez, R.; Zhong, J.; de Graaf, C.; Rodriguez-Fortea, A.; Poblet, J. M.; Echegoyen, L.; Feng, L.; Chen, N. U$_2$@$I_h(7)$-C$_{80}$: Crystallographic Characterization of a Long-Sought Dimetallic Actinide Endohedral Fullerene. *J. Am. Chem. Soc.* **2018**, *140*, 3907−3915.

(50) Zhao, P.; Yang, T.; Guo, Y. J.; Dang, J. S.; Zhao, X.; Nagase, S. Dimetallic Sulfide Endohedral Metallofullerene Sc$_2$S@C$_{76}$: Density Functional Theory Characterization. *J. Comput. Chem.* **2014**, *35*, 1657−1663.

(51) Zheng, H.; Zhao, X.; He, L.; Wang, W. W.; Nagase, S. Quantum Chemical Determination of Novel C$_{82}$ Monometallofullerenes Involving a Heterogeneous Group. *Inorg. Chem.* **2014**, *53*, 12911−12917.

(52) Yang, T.; Zhao, X.; Nagase, S. Quantum Chemical Insight of the Dimetallic Sulfide Endohedral Fullerene Sc$_2$S@C$_{70}$: Does It Possess the Conventional D_{5h} Cage? *Chem. Eur. J.* **2013**, *19*, 2649−2654.

(53) Frisch, M. J.; Trucks, G. W.; Schlegel, H. B.; Scuseria, G. E.; Robb, M. A.; Cheeseman, J. R.; Scalmani, G.; Barone, V.; Petersson, G. A.; Nakatsuji, H.; Li, X.; Caricato, M.; Marenich, A. V.; Bloino, J.; Janesko, B. G.; Gomperts, R.; Mennucci, B.; Hratchian, H. P.; Ortiz, J. V.; Izmaylov, A. F.; Sonnenberg, J. L.; Williams-Young, D., Ding, F.; Lipparini, F.; Egidi, F.; Goings, J.; Peng, B.; Petrone, A.; Henderson, T.; Ranasinghe, D.; Zakrzewski, V. G.; Gao, J.; Rega, N.; Zheng, G.; Liang, W.; Hada, M.; Ehara, M.; Toyota, K.; Fukuda, R.; Hasegawa, J.; Ishida, M.; Nakajima, T.; Honda, Y.; Kitao, O.; Nakai, H.; Vreven, T.; Throssell, K.; Montgomery, J. A., Jr.; Peralta, J. E.; Ogliaro, F.; Bearpark, M. J.; Heyd, J. J.; Brothers, E. N.; Kudin, K. N.; Staroverov, V. N.; Keith, T. A.; Kobayashi, R.; Normand, J.; Raghavachari, K.; Rendell, A. P.; Burant, J. C.; Iyengar, S. S.; Tomasi, J.; Cossi, M.; Millam, J. M.; Klene, M.; Adamo, C.; Cammi, R.; Ochterski, J. W.; Martin, R. L.; Morokuma, K.; Farkas, O.; Foresman, J. B.; Fox, D. J. *Gaussian 16*, rev. A.03; Gaussian, Inc.: Wallingford, CT, 2016.

(54) Lu, T.; Chen, F. W. Multiwfn: A Multifunctional Wavefunction Analyzer. *J. Comput. Chem.* **2012**, *33*, 580−592.

(55) Mercado, B. Q.; Stuart, M. A.; Mackey, M. A.; Pickens, J. E.; Confait, B. S.; Stevenson, S.; Easterling, M. L.; Valencia, R.; Rodriguez-Fortea, A.; Poblet, J. M.; Olmstead, M. M.; Balch, A. L. Sc$_2(\mu_2$-O$)$ Trapped in a Fullerene Cage: The Isolation and Structural Characterization of Sc$_2(\mu_2$-O$)$@C$_s(6)$-C$_{82}$ and the Relevance of the Thermal and Entropic Effects in Fullerene Isomer Selection. *J. Am. Chem. Soc.* **2010**, *132*, 12098−12105.

(56) Kobayashi, K.; Nagase, S. Bonding Features in Endohedral Metallofullerenes. Topological Analysis of the Electron Density Distribution. *Chem. Phys. Lett.* **1999**, *302*, 312−316.

(57) Popov, A. A.; Dunsch, L. Bonding in Endohedral Metallofullerenes as Studied by Quantum Theory of Atoms in Molecules. *Chem. Eur. J.* **2009**, *15*, 9707−9729.